

Université de Mons
Faculté Polytechnique – Service de Mécanique Rationnelle, Dynamique et Vibrations
31, Bld Dolez - B-7000 MONS (Belgique)
065/37 42 15 – georges.kouroussis@umons.ac.be



D. P. Connolly, K. E. Vogiatzis, G. Kouroussis, A hybrid experimental-numerical approach to predict ground vibrations from localised railway defects, *Proceedings of the 14th International Railway Engineering Conference (Railway Engineering 2017)*, Edinburgh (UK), June 21-22, 2017.

A HYBRID EXPERIMENTAL-NUMERICAL APPROACH TO PREDICT GROUND VIBRATIONS FROM LOCALISED RAILWAY DEFECTS

David P Connolly,
Institute for Infrastructure and Environment
Heriot Watt University
EH14 1AS
UK
d.connolly@hw.ac.uk

Konstantinos E Vogiatzis
Laboratory of Transportation Environmental
Acoustics,
University of Thessaly,
Greece

Georges Kouroussis
Department of Theoretical Mechanics, Dynamics and Vibrations,
University of Mons,
Belgium

KEYWORDS: Hybrid modelling, ground vibration, urban tram, rail defects, joint, switch, crossing

ABSTRACT

Local railway defects such as joints generate large forces when excited by a passing train. This is particularly a problem in urban environments where trams traverse lines densely populated with defects. This paper proposes a hybrid experimental-numerical approach to predict the ground-borne vibrations caused by these singularities. Firstly, a multibody train-track numerical model is used to generate the force densities caused when a tram passes over a variety of defects. These densities are then coupled with experimental transfer functions, thus allowing for the effect of singular defects to be included in vibration studies. Using the proposed methodology, analysis is performed into the effect of different types of defect on vibration levels at several physical sites on a European tram network.

INTRODUCTION

Ground-borne vibration from railways is a nuisance in urban areas. There are two primary approaches to evaluate vibration: numerical modelling [1], [2], [3] and physical testing [4], [5]. Numerical modelling is suitable for performing parametric studies and for simulating situations where input parameters are well defined. However, for the case of urban railways, the uncertainties caused by complex topography and infrastructure arrangements (e.g. buried services) mean that it is often best suited for scoping purposes only. In practise, physical testing is more commonly used and allows for the determination of transfer functions between a source (i.e. potential railway) and a receiver (i.e. existing building) [4], [5]. Physical testing procedures are typically concerned with determining a line-source transfer mobility, which accounts for the contribution of a long length of train traversing a (relatively) smooth track. However, in urban environments, tracks are densely populated with localised rail discontinuities (e.g. rail joints, switches and turnouts), which generate vibration levels much larger than a horizontally continuous track.

Many ground-borne vibration complaints in urban environments are due to local rail and wheel surface defects (e.g. switches, rail joints, etc). Therefore the first step in analysing this problem is to understand wheel/rail interaction at the defect location. In an attempt to do this, Zhao et al. [3] evaluated the wheel/rail impact forces at the location of local rail surface defect zones using a three-dimensional finite element model. They also evaluated the resulting dynamic forces at the discrete supports of the rail under different train speeds. Alternatively, Grossoni et al.[6] performed a parametric study to understand the dynamic behaviour of a rail joint and the influence of track and vehicle parameters on track dynamics. Mandal et al. [7] also studied the impact forces on wheels at dipped rail joints, showing that they were of very short duration, of high magnitude and with high-frequency content.

Kouroussis et al. [8] showed that models based only on vertical wheel/rail forces fail to predict horizontal ground-borne vibrations generated by local rail joints. Kouroussis [9] further developed a

multibody vehicle/track model to account for track discontinuities. This model was capable of calculating the impact forces generated at a variety of rail joints or other localised defects with different dimensions.

The objective of this paper is to couple a newly developed discontinuity vibration prediction model with in-situ physical testing procedures. The final approach will be suitable for calculating the vibration response of any rail defect, for any case of new railway line. First the physical testing procedure required to couple with the numerical model is described. Then the numerical model is presented, followed by a strategy to couple both physical and numerical models. Finally a case study is performed in on a tram line and the effect of train speed and defect characteristics is investigated. The aim of the tool is to provide a method that improves the accuracy of railway vibration assessment while minimising costs.

HYBRID MODELLING APPROACH

Overview

For ground vibration assessment on existing lines, in situ monitoring is often used. For new lines however, physical testing is usually preferred to determine the transfer characteristics of the soil because it can capture the highly heterogeneous nature of the soil. These physical test results are coupled with the track response via either historical measurements or numerical simulations. A challenge with the case of rail discontinuities is that, due to their highly variable nature, historical measurements are rarely available and numerical simulations can be complex.

Physical modelling (vibration propagation)

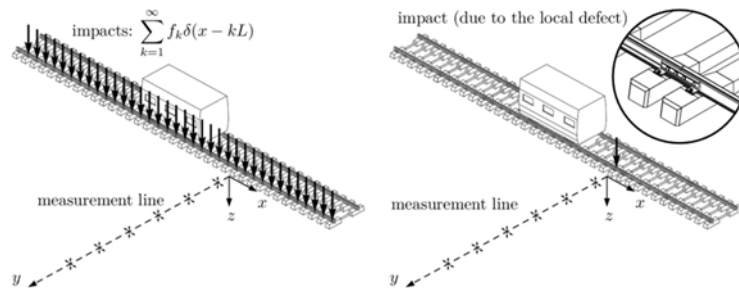


Figure 1 - The effect of vehicle passing over a railtrack. Left: (a) for distributed source, Right: (b) for local source of excitation. The bold arrows represent the main contribution of the vehicle passing. This corresponds to the expected excitation to be produced by equivalent excitations

Ground vibration near railway lines is caused by dynamic train loads, which depend on the nature of the interaction between the railway vehicle and the track. As discussed by Kouroussis et al. [10] ground-borne vibrations generated by railroads can be categorised depending upon the excitation mechanism:

- If the track is characterised by a very high quality rolling surface, the effect generated by the moving of axle loads can be considered as static or quasi-static, thus effecting static track displacement. The term “quasi-static” is generally used where the vehicle’s speed is significantly lower than the critical track [11] and soil speeds [12].
- If surface imperfections play a role on wheel/rail forces, then a dynamic excitation is added to the static contribution. In the case of low speeds (up to 80 km/h, as in an urban area), the dynamic excitation has a dominant influence on ground vibration levels.

In the case of a perfect track surface or where there are few irregularities along the track alignment, quasi-static effects dominate ground vibration. Due to the track invariance along the direction x , it is assumed that the effect of a moving wheelset j on a track/soil system can be represented by:

$$f_{exc,j} = \sum_{k=1}^{\infty} f_k \delta(x - kL)$$

where f_k is the force acting through the k^{th} sleeper interface at each distance L (sleeper spacing). The resulting vibrations at different distances from the track result from the summation of the effects of each force f_k in the near-field (Figure 1) and are often called line source vibration. In practice, the forces acting on sleepers far from the receptor have a negligible influence on the resulting vibration level, so the above equation becomes:

$$f_{exc,j} = \sum_{k=1}^m f_k \delta(x - kL)$$

In the case of a local defect, the ground vibration near railway lines is the result of the interaction of the railway vehicle and the track irregularity (Figure 1). In addition, if the vehicle speed is low (e.g. light transit vehicles, like trams or metros) typically this type of line will also have a relatively high density of singular rail surface defects. In this case, dynamic track deflection dominates ground wave generation meaning it is reasonable to consider a single force acting on the wheel/rail defect contact point as the only contributor to railway vibration. Therefore,

$$f_{exc,j} = f_{wheel/rail}$$

represents the force acting at the wheel/rail interface when a wheelset j is in contact with the local defect.

A physical testing procedure, such as the technique developed by Nelson and Saurenman [5], is often used for predicting ground borne noise and vibration caused by railway vehicles. The main focus of this tool is the estimation of ground-borne noise and vibration between 6.3 and 200 Hz in residential areas near at-grade and subway track. It does so by calculating the line transfer mobility, defined as a function of the frequency f ,

$$M_{L,i} = 10 \log_{10} \left(d \sum_{j=1}^l 10^{M_{ij}/10} \right)$$

It is obtained via the superposition of l point transfer mobilities M_{ij} between several points j ($j:1 \rightarrow l$) of the rail, spaced of distance d , and the studied receptor response x_i , and the force density L_F obtained from tests [4] (or numerical calculations [13]). The resulting vibration is calculated at distance y_i from the track to predict the vibration velocity level

$$L_{V,i} = L_F + M_{L,i}$$

The basis of this method is the measurement of a single source transfer mobility function between various points i on a system. This function gives the dynamic transfer characteristics (in the frequency domain [14]) between two points of the system — the soil velocity response $X_i(f)$ and the force $F_j(f)$ acting at the soil surface. A single source transfer mobility is theoretically defined by

$$M_{ij}(f) = 10 \log_{10} \left(\frac{X_i(f)}{F_j(f)} \right)$$

When considering low speed vehicles and in the presence of local defects, one point transfer mobility (or a small number of point transfer mobilities) is sufficient to evaluate ground wave propagation, (i.e. by combining the latter two equations). This situation is very common in urban environments and thus the present study focuses solely on this problem.

Numerical modelling (vibration generation)

Vehicle/track/foundation modelling

The structure of the vehicle/track/foundation model is summarised in Figure 2. It is derived from the model of Zhai and Sun [15] and consists of a classical multibody vehicle model, coupled to a finite element/lumped mass track model. The latter lies on a foundation represented by a coupled lumped mass (CLM) model. The foundation is thus defined by its mass, damping, and stiffness matrices, constructed from its mechanical and geometrical properties. This offers a way to accurately predict the track response

at low frequencies where the foundation plays an important role, by creating a more realistic coupling [16], [17].

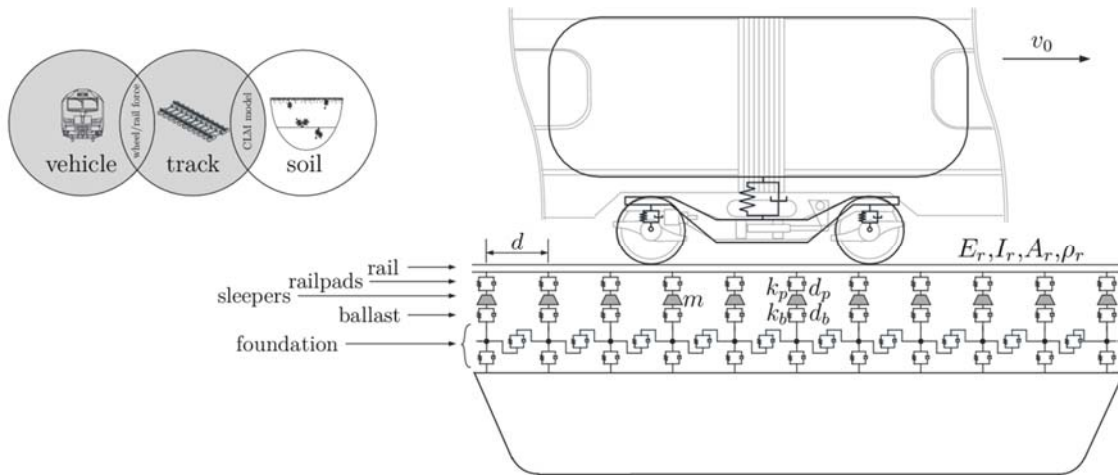


Figure 2 - Vehicle/track/foundation simulation [18]

The track and vehicle subsystems are coupled via the wheel/rail contact forces, explicitly considered as non-linear, and depending on the position of wheel and its contact with the rail:

$$F_{wheel/rail,i} = K_{Hz}(z_{wheel,i} - z_{rail}(x_j) - h_{defect})^{1.5}$$

This connection force is more realistic than a simple linear spring since it is derived from Hertz's theory, depending on the vertical position $z_{wheel,i}$ of the wheel and the corresponding vertical displacement $z_{rail}(x_j)$ at the rail at coordinate, x_j . K_{Hz} is the Hertz's coefficient (in $Nm^{2/3}$ — different from the Hertz's stiffness). The vertical dynamic response of the vehicle/track subsystem due to the rail irregularity h_{defect} is therefore calculated using the geometry of the studied local defect (represented by an analytical function).

Modelling local defects and singularities

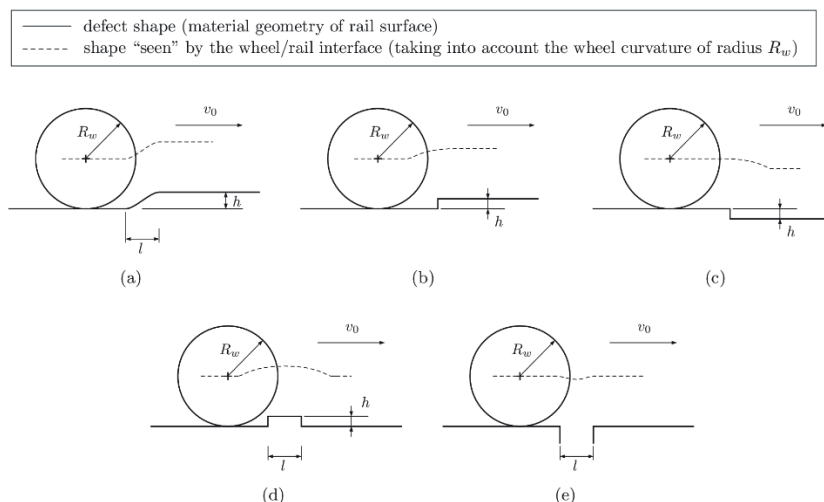


Figure 3 - Mathematical modelling of local rail and wheel surface defects: (a) ramp, (b) step-up joint, (c) step-down joint, (d) pulse joint and (e) negative pulse joint [9]

Figure 3 presents the singular rail and wheel surface defects studied in this paper. Each defect is characterized by its length l and its height h and is defined using a specific shape seen by the wheel running at a speed v_0 (assumed to be constant). Each of these defect types can be modelled as a single

dynamic excitation at the wheel/rail defect contact point. Although a small number of alternative defects exist, such as wheel flats (which induce a series of periodic impacts), these are outside the scope of this work.

Coupling of experimental and numerical approaches

The wheel/rail contact forces $F_{wheel/rail,i}$ acting at the defect location are saved during the simulation and are then combined with the measured transfer mobility functions. This allows for the calculation of ground vibration at the desired locations. Logically, according to the basic principles explained in Section 2, the dynamic part of wheel/rail force acting on the specific rail location (on the defect) is required, and the quasi-static component can be neglected. Practically, it is assumed that a small part of rail location around the defect considered, in order to take into account the whole force shape. With the source mobility function M_{ij} defined previously, the simulated force density L_F , obtained using the discrete Fourier transform of $F_{wheel/rail}$ is:

$$L_F = 10 \log_{10} \left(DFT(F_{wheel/rail}) \right)$$

which provides the information necessary to calculate the vibration velocity level $L_{V,i}$ defined by

$$L_{V,i} = L_F + M_{i,j}$$

An inverse Fourier transform then allows for time history representation.

CASE STUDY

Collection Of Experimental Data

Experimental data was collected from a combination of ballasted and slab tracks, designated site 1 to site 14, across Brussels. Accelerometers were placed along a profile perpendicular to the track, allowing the measurement of the vertical soil response $x_i(t)$. The first accelerometer was placed close to the track (tram site edge) and the others at distant points of interest (e.g. sensitive building, foundation walls of dwelling, ...), while maintaining a similar distance from the track/foundation where possible. A falling mass was used to excite the track at the rail head, at the localized singular defect. It consisted of multiple masses of 12.5 kg, and an elastomer support allowing for the physical filtering of the desired frequency range (up to 100–150 Hz). The maximum mass was 52 kg and could be dropped from a maximum height of 1.5 m.

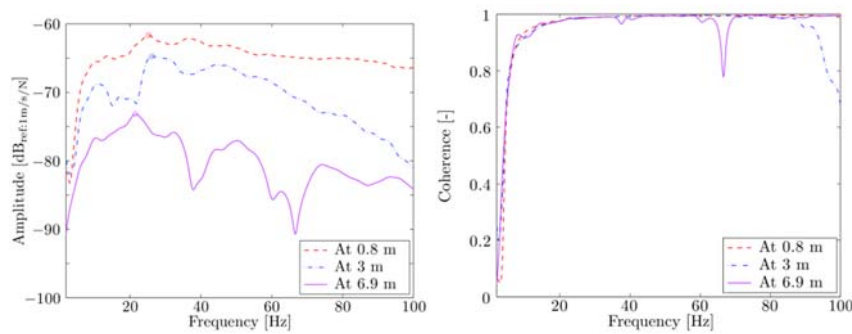


Figure 4 - Transfer mobility functions M_{ij} for site 6 (ballasted track). Left: (a) magnitude, Right: (b) coherence

Figure 4 presents an example of calculated transfer mobility functions (here for site 6, ballasted track). Coherence curves (Figure 4) are also plotted in order to define the frequency range free from measurement errors and it shows a relatively good accuracy for the results in the frequency range between 10 and 90 Hz. A maximum amplitude is found for frequencies in the range 21–23 Hz depending on the track/soil configuration. Dynamic excitation generated within the track is both filtered and dampened by the soil as it propagates. This shows an attenuation with the distance over the entire frequency range -

between track and building foundation, a difference of approximately 10–15 dB is observable. Similar trends were also found for the alternative sites.

Computation Of Numerical Data

The T2006 tram was used as a reference for the various aforementioned sites and local defects. Developed by Bombardier Transport, this multicar tramway is composed of three car bodies and characterized by a low floor design, meaning the motors are mounted directly inside the wheels and the bogies have independent rotating wheels. The multibody model thus limits the vehicle dynamics to pitch and bounce motions. The proposed model includes resilient wheels characterized by a soft rubber layer, reducing the impact of high unsprung masses on the rail. Kouroussis et al. [19] analysed in-depth the vehicle dynamics coupled to the track and showed that, when the tram passes over localized defects, it generates high level vibrations characterised by several vehicle modes. All the simulations were computed considering a small portion of the track ($N = 40$ and $N_n = 2$, for a track of 14 m length — this consisted of a 124 degrees-of-freedom track model, plus a 16 degrees-of-freedom vehicle model). The dynamic characteristics of the track were similar to those of [19].

Figure 5 presents some examples of calculated wheel/rail forces obtained using the vehicle/track/foundation model. The passing of the tram at a constant speed of $v_0 = 30$ km/h on a ramp and a pulse defect is shown as an illustrative example. The impact of each wheel is clearly visible: each axle crosses the defect at times $t = 0.98$ s, $t = 1.19$ s, $t = 1.89$ s, $t = 2.09$ s, $t = 2.79$ s and $t = 2.99$ s, with strong oscillations after each impact. This corresponds to a signal frequency of approximately 16 Hz and is associated with the vehicle's bogie bounce mode. Despite having a similar height, both defects do not generate the same force amplitude, the latter being more important for the pulse defect, which is shorter and more discontinuous than the ramp defect. The same simulations were computed for the other defects and found to be consistent with the findings in [8].

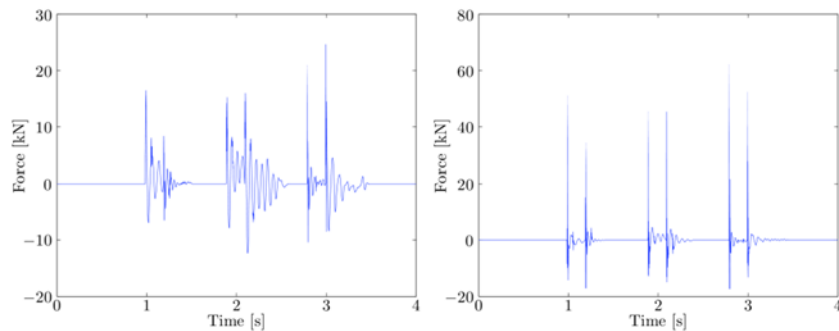


Figure 5 - Left: Calculated wheel/rail forces acting on defect location for a T2006 tram running at 30 km/h on a ramp defect ($h = 1$ m; $l = 0.05$ m). Right: Calculated wheel/rail forces acting on defect location for a T2006 tram running at 30 km/h on a pulse joint defect ($h = 1$ mm; $l = 5$ mm).

RESULTS

Figure 6 shows the ground vibration results for all defects with similar heights (1 mm) and lengths (5 mm, except for the ramp defect where $l = 0.05$ m is considered), for site 1. It is seen that that the vibration duration is similar however each wheel passing on a specific defect generates different vibration characteristics (both in geometry and magnitude). When computing the time histories, attention was paid to the causality of the response, due to the use of the inverse discrete Fourier transform, and the results were verified in all cases. As expected, the ramp defect generated lower vibration levels than the other

cases, except for the negative pulse joint. This was due to its short length, resulting in a lower height than the other cases. When the wheel is in contact with the first rail edge, it moves down until it is in contact with the second edge, thus meaning that for a length $l = 0.005$ mm, the apparent height is only 0.01 mm (compared to $h = 1$ mm for the other defect cases).

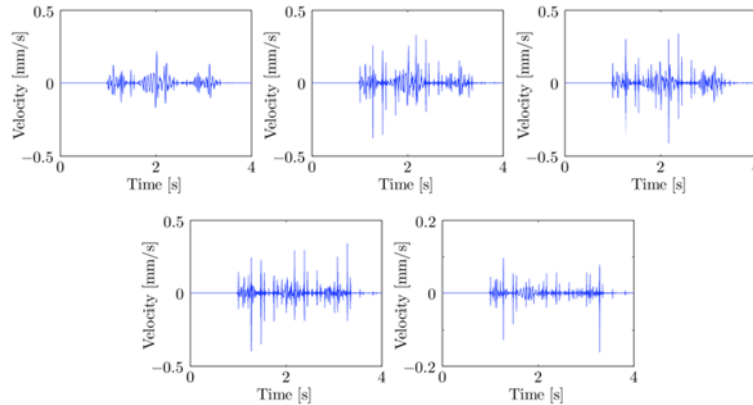


Figure 6 - Time histories of vibration velocity predicted at 13 m from the track (site 1) for a tram T2006 running at 30 km/h as a function of the defect type: (a) ramp ($h = 1$ mm; $l = 0.05$ m), (b) step-up joint ($h = 1$ mm), (c) step-down joint ($h = 1$ mm), (d) pulse joint ($h = 1$ mm; $l = 5$ mm) and (e) negative pulse joint ($l = 5$ mm).

Figure 7 shows the vibration levels for a theoretical pulse joint at each experimental site for a receiver located between 6.9 m and 13 m. A direct comparison of attenuation was not possible because the sensors were placed at different distances, however a few trends are noticeable. Firstly, the track installation has a strong influence of the vibratory impact on neighbour buildings. Comparing the results between track types, in general it is seen that slab tracks (sites 7 to 14) present improved vibration isolation than classic ballasted tracks (sites 1 to 6). Other findings observed from all the site results revealed that:

- The mean vibration level at the foundation location varies with measurement site. The maximum level does not exceed 5 mm/s, which usually represents a threshold for such buildings. Sites 9, 7, 3 and 2 present, in that order, higher *PPV*. Site 1 (with the increased track-foundation distance) does not present elevated vibration levels.
- No notable difference between ballasted track vibration levels, including concrete (sites 1 and 2) or wood sleepers (sites 3 to 6), was found.
- The only site with floating slab, site 9, generated the highest level of vibrations, however, only two measurement locations were considered.
- Regarding slab track sites 10-14 (same track-foundation distance of 7.9 m), the vibration level was relatively similar, except for site 10.

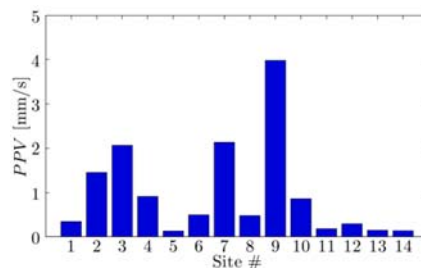


Figure 7 - Predicted *PPV* as a function of all the studied sites for a T2006 tram running at 30 km/h on a pulse joint defect ($h = 1$ mm; $l = 5$ mm).

Effect Of Tram Speed

Table 1 shows the effect of varying tram speed (in the range 20–80 km/h) on PPV for all 14 sites in the presence of a step-up joint. Similar trends to previously are observed regarding the different sites. For each site, *PPV* decreases when the tram changes speed from 50 to 60 km/h (except site 5 where this phenomenon occurs from 60 to 70 km/h). This local change is important according to the site, however, it is difficult to explain the cause of these specific differences. One drawback of using field mobility functions is that the subsurface data and configuration is never known.

	Speed [km/h]	20	30	40	50	60	70	80
site 1 (at 13 m from the track)	<i>PPV</i> [mm/s]	0.29	0.37	0.63	0.85	0.58	1.36	1.39
site 2 (at 2.7 m from the track)	<i>PPV</i> [mm/s]	1.17	1.34	2.22	2.97	1.92	4.43	4.23
site 3 (at 8 m from the track)	<i>PPV</i> [mm/s]	1.58	1.86	3.23	4.12	2.66	6.62	5.25
site 4 (at 5.3 m from the track)	<i>PPV</i> [mm/s]	0.54	0.72	0.99	0.88	1.08	1.02	1.63
site 5 (at 7.8 m from the track)	<i>PPV</i> [mm/s]	0.14	0.16	0.21	0.36	0.17	0.38	0.38
site 6 (at 6.9 m from the track)	<i>PPV</i> [mm/s]	0.31	0.45	0.71	0.95	0.59	1.46	1.41
site 7 (at 11 m from the track)	<i>PPV</i> [mm/s]	1.44	1.84	3.29	4.00	2.85	6.55	6.06
site 8 (at 4.8 m from the track)	<i>PPV</i> [mm/s]	0.38	0.49	0.66	0.46	0.57	0.63	0.89
site 9 (at 8.7 m from the track)	<i>PPV</i> [mm/s]	2.97	3.63	6.68	8.04	5.17	12.62	11.61
site 10 (at 7.9 m from the track)	<i>PPV</i> [mm/s]	0.60	0.81	1.48	1.75	1.21	2.75	2.56
site 11 (at 7.9 m from the track)	<i>PPV</i> [mm/s]	0.18	0.22	0.28	0.39	0.24	0.67	0.78
site 12 (at 7.9 m from the track)	<i>PPV</i> [mm/s]	0.26	0.26	0.45	0.53	0.37	0.84	0.87
site 13 (at 7.9 m from the track)	<i>PPV</i> [mm/s]	0.15	0.17	0.27	0.28	0.18	0.48	0.47
site 14 (at 7.9 m from the track)	<i>PPV</i> [mm/s]	0.13	0.14	0.21	0.24	0.17	0.41	0.38

Table 1 - Predicted *PPV* as a function of speed for a T2006 tram running on a step-up joint ($h = 1$ mm) and for all the studied sites.

Defect size was also investigated, with Figure 8 showing the results of an analysis for a T2006 tram running at 50 km/h on a step-up joint and a step-down joint. Both vibration *PPV* and V_{dB} values (according to [4]) are compared, in order to have an overall view of the vibration peak (*PPV*) and of the vibration energy (V_{dB}). In a general way, the vibration levels increase with defect size. A positive relationship between defect size and vibration level is found (except for the *PPV* vs. step-down joint where the values exhibit localised peaks, however without a strong positive trend)). It is also interesting to note that the step-up joint and the step-down joint yield very different vibration levels (both *PPV* and V_{dB} values) even though the defect shapes are identical but opposite in shape. The non-linear effects at the wheel/rail contact are evident since the two defects (same wheel/rail contact definition) induce different ground vibration levels. This effect was discussed in [8], demonstrating that the vehicle dynamics have a strong influence on the vibration levels for such cases.

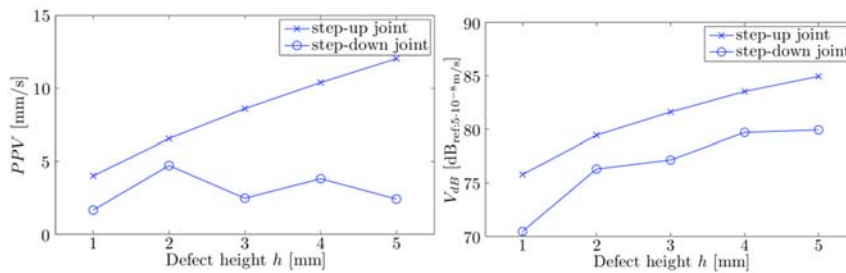


Figure 8 - Predicted vibration levels as a function of the defect size for site 7 for a T2006 tram running at 50 km/h. Left: (a) a step-up joint, (b) a step-down joint

CONCLUSIONS

Railway-induced ground vibrations can cause negative effects to people/structures located near lines. One of the main sources of these vibrations is from the large vehicle forces generated when the train wheels impact local defects (e.g. switches/crossings). These defects occur frequently in densely populated areas due to the complex track infrastructure arrangements associated with urban lines. Furthermore, the vibration propagation path and receiver configurations are also complex due to rapid changes in terrain

and building layout. These complexities make numerical modelling challenging and therefore this paper presented a combined experimental-numerical prediction approach to overcome this. Firstly an experimental method to determine the transfer mobility between source and receiver was described. Then a vehicle-track numerical model was outlined, that was well suited to simulating the forces generated when vehicle wheels impact a rail discontinuity. The two modelling approaches were combined to enable the prediction of ground-borne vibration propagation from a variety of defects into nearby buildings. The procedure is capable of modelling any type of vehicle, speed and defect. Finally, a case study was used to show the capability of the modelling approach. To do so, an experimental campaign was undertaken on a tram line in Belgium and the results coupled with numerical simulations of a T2006 tram. The effect of tram speed was then investigated.

REFERENCES

- [1] L. Auersch, "Vibration of buildings on pile groups due to railway traffic – finite- element boundary-element , approximating and prediction methods L Auersch," no. 2, 2010.
- [2] D. López-Mendoza, A. Romero, D. P. Connolly, and P. Galvín, "Scoping assessment of building vibration induced by railway traffic," *Soil Dyn. Earthq. Eng.*, vol. 93, no. June, pp. 147–161, 2017.
- [3] G. Kouroussis, O. Verlinden, and C. Conti, "Free field vibrations caused by high-speed lines: Measurement and time domain simulation," *Soil Dyn. Earthq. Eng.*, vol. 31, no. 4, pp. 692–707, Apr. 2011.
- [4] Federal Railroad Administration, "High-Speed Ground Transportation Noise and Vibration Impact Assessment. U.S. Department of Transportation," 2012.
- [5] J. Nelson and H. Saurenman, "A prediction procedure for rail transportation groundborne noise and vibration," *Transp. Res. Rec. J. Transp. Res. Board*, no. 1143, pp. 26–35, 1987.
- [6] I. Grossoni, S. Iwnicki, Y. Bezin, and C. Gong, "Dynamics of a vehicle–track coupling system at a rail joint," *J. rail rapid transit*, vol. 229, no. 4, pp. 364–374, 2015.
- [7] N. K. Mandal, M. Dhanasekar, and Y. Q. Sun, "Impact forces at dipped rail joints," *J. rail rapid transit*, vol. 230, no. 1, pp. 271–282, 2016.
- [8] G. Kouroussis, D. P. Connolly, G. Alexandrou, and K. Vogiatzis, "Railway ground vibrations induced by wheel and rail singular defects," *Veh. Syst. Dyn.*, pp. 1500–1519, 2015.
- [9] G. Kouroussis, D. P. Connolly, G. Alexandrou, and K. Vogiatzis, "The effect of railway local irregularities on ground vibration," *Transp. Res. Part D Transp. Environ.*, vol. 39, pp. 17–30, 2015.
- [10] G. Kouroussis, D. P. Connolly, and O. Verlinden, "Railway induced ground vibrations - a review of vehicle effects," *Int. J. Rail Transp.*, vol. 2, no. 2, pp. 69–110, 2014.
- [11] P. K. Woodward, J. Kennedy, O. Laghrouche, D. P. Connolly, and G. Medero, "Study of Railway Track Stiffness Modification by Polyurethane Reinforcement of the Ballast," *Transp. Geotech.*, vol. 1, pp. 214–224, 2014.
- [12] S. B. Mezher, D. P. Connolly, P. K. Woodward, O. Laghrouche, J. Pombo, and P. A. Costa, "Railway critical velocity - Analytical prediction and analysis," *Transp. Geotech.*, 2015.
- [13] H. Verbraeken, G. Lombaert, and G. Degrande, "Verification of an empirical prediction method for railway induced vibrations by means of numerical simulations," *J. Sound Vib.*, vol. 330, no. 8, pp. 1692–1703, Apr. 2011.
- [14] E. Bovey, "Development of an impact method to determine the vibration transfer characteristics of railway installations," *J. Sound Vib.*, vol. 87, no. 2, pp. 357–370, 1983.
- [15] W. Zhai and X. Sun, "A detailed model for investigating vertical interaction between railway vehicle and track," *Veh. Syst. Dyn.*, vol. 23, pp. 603–615, 1994.
- [16] G. Kouroussis and O. Verlinden, "Prediction of railway ground vibrations: Accuracy of a coupled lumped mass model for representing the track/soil interaction," *Soil Dyn. Earthq. Eng.*, vol. 69, no. 2015, pp. 220–226, 2015.
- [17] A. Colaço, P. A. Costa, and D. P. Connolly, "The influence of train properties on railway ground vibrations," *Struct. Infrastruct. Eng.*, pp. 1–18, 2015.

- [18] B. Olivier, D. P. Connolly, P. Alves Costa, and G. Kouroussis, "The effect of embankment on high speed rail ground vibrations," *Int. J. Rail Transp.*, vol. 4, pp. 229–246, 2016.
- [19] G. Kouroussis, O. Verlinden, and C. Conti, "Efficiency of resilient wheels on the alleviation of railway ground vibrations," *Proc. Inst. Mech. Eng. Part F J. Rail Rapid Transit*, vol. 226, no. 4, pp. 381–396, Dec. 2011.